Effect of High and Low Storage Temperatures, Storage Duration and Varying Depth of Discharge on Coin Cell SOH Degradation

Pradeep Lall
Auburn University
NSF-CAVE3, Electronic Research Center,
Department of Mechanical Engineering,
Auburn, AL. 36849.
Email – lall@auburn.edu

Ved Soni
Auburn University
NSF-CAVE3, Electronic Research Center,
Department of Mechanical Engineering,
Auburn, AL. 36849.

Guneet Sethi
Amazon Lab 126,
Sunnyvale, CA.

Kok Yiang
Amazon Lab 126,
Sunnyvale, CA.

Abstract – **Portable consumer electronics devices continue to be one of electronics high-demand items, with rising interest in such products recently. Li-Ion batteries are the most popular power source choice of these products owing to a combination of high specific energy and specific power. In consumer electronics products, these batteries are generally employed in their coin form factor in biomedical devices, sensors, wireless earbuds, etc. These developments have boosted the research effort on Li-Ion power sources, and a major part of this effort is the prognostics of Li-Ion battery state of health (SOH) and predicting its remaining useful life. The ubiquitous use-parameters of batteries in modern consumer electronics devices are charging currents i.e. C-rates, operating temperatures, depths of charge, etc. Depth of discharge of the battery is another use parameter that has been explored in the current study. Two levels of depth of discharge have been tested and their SOH degradation profiles have been included in the SOH estimation dataset. Apart from this, calendar ageing of the battery due to storage at high and low temperatures for long durations is another common cause leading to battery SOH degradation. The storage scenario generally occurs during the manufacturing and retailing stage of the battery rather than at the end-usage stage. To study the degradation in state of health caused due to such calendar ageing, the coin cells in this study were subjected to storage at three temperatures (i.e., -10°C, 40°C, 60°C) for three durations (45 days, 120 days, 180 days). The pre-aging and post-aging capacities were measured and the difference between them was correlated with the harshness of the particular storage condition. In addition, after storage, the samples were subjected to accelerated life testing to evaluate the effect of storage on their SOH degradation rate. Thus, the SOH estimation models developed for two different coin cells in our previous study have been appended with the data generated during this study. Apart from this, calendar-ageing models have also been developed for the battery samples that were aged using different storage conditions.**

Keywords - capacity degradation, state of health, consumer electronics, SOH modelling, RUL modelling, li-ion battery, coin cell.

I. INTRODUCTION

Owing to its excellent combination of high specific energy and high specific power, the lithium-ion battery is the most popular electrical energy storage technology in current portable consumer electronics products [1][2]. Because of increasing miniaturization, applications like as smartcards, radio frequency-based identification tags (RFID), and biomedical sensors [3][4][5] have adopted this battery technology in either its coin or pouch form factor. Over the last two decades, a plethora of experimental research on lithium-ion battery degradation has been published, in which power sources have been subjected to accelerated life cycling in combination with a variety of operating conditions such as high currents, temperatures, and charge/discharge depth variations, among others. [6][7][8][9].

The identification of electrochemical failure modes of batteries in order to optimize battery design while enhancing safety, and the development of methods to estimate battery capacity degradation in order to determine its end-of-life (EOL), also known as battery health prognostics, are two of the main goals of lithium-ion battery degradation research. The battery failure mode research has matured, but battery health prognostics is currently gaining traction thanks to a slew of artificial intelligence-based methodologies being applied to handle this complex challenge. Building a mathematical model for calculating the current 'state of health' and hence predicting the remaining usable life (RUL) of a battery as a function of the number of charge-discharge cycles and the operating circumstances it has been subjected to is typical of battery health prognostics. As shown in [10], the state of health of a battery is defined as the ratio of its current capacity to its nominal capacity converted to a percentage form (see (1)). When a battery's capacity has declined to 80% of its nominal value, it is deemed to have reached its end of life [10].

$$\text{State of Health (SOH)} = \frac{\text{Battery Capacity}}{\text{Rated Capacity}} * 100 \quad (1)$$

Lithium-ion batteries accumulate degradation over their lifetime which can be classified into two categories: calendar ageing which results from storing the battery idle without either charging or discharging it, and the second is cycle ageing, where the battery is continuously charged and discharged. In our previous study [11], we investigated the cycle ageing behavior of two Li-ion coin cells with respect to various use parameters such as the charge and discharge currents, operating

temperature, and depth of charge. This study will primarily focus on calendar ageing and the effect of storage duration and temperatures on the capacity degradation of the same two coin cells. Furthermore, after the calendar ageing of these cells, they will also be subjected to an accelerated charge-discharge cycling test for multiple cycles to investigate their SOH degradation behavior after calendar ageing. Also, to add to the previous cycle ageing study, we have performed a depth of discharge testing dataset on pristine cells to more completely investigate the effect of cycling between various SOC limits on the li-ion battery. As in the previous study, the goal of this study would be to develop an empirical nonlinear regression model to estimate the capacity drop after storage at various conditions. Following are some of the empirical models that have been developed previously. Ref [12] performed calendar ageing of li-ion batteries for temperatures ranging between 0 - 60C and SOCs ranging between 0 – 100%. The total ageing duration was 18 months, and the batteries were periodically investigated for their total capacity reading after every one month of ageing. Equation (2) and (3) represents the model for the degradation rate where z_{cal} is a dimensionless constant, B_{cal} is a pre-exponential factor and $E_{a,cal}$ is the activation energy.

$$\frac{dQ_{loss}^{cal}}{dt} = z_{cal} k_{cal} \left(\frac{Q_{loss}}{k_{cal}}\right)^{1-\frac{1}{z_{cal}}} \tag{2}$$

$$k_{cal} = B_{cal} \exp\left(-\frac{E_{a,cal}}{RT}\right) \tag{3}$$

Ref [13] performed calendar ageing test on Li-ion batteries with NMC cathode with 350 mAh capacity at 60C at five different SOC levels ranging from 50% to 100% SOC. Their results indicated that the ageing performed at higher SOC levels such as 90% and 100% was higher and more distinguished rather than that performed at lower SOC levels (80%, 70%, 50%). Following is the calendar ageing model devised by them wherein they model the capacity fade due to calendar ageing to have a linear relation to storage duration (see (4) and (5)). The term Ca in the model takes into account the effect of temperature and SOC.

$$Q_{loss}(t) = C_a * t \tag{4}$$

$$C_a = AT^n * \exp\left(\begin{array}{l} \frac{-E_a}{kT} \\ \quad + B_1 f_1(SOC) \\ \quad + B_2 f_2(SOC) + \ldots \end{array}\right) \tag{5}$$

Ref [14] proposed a calendar ageing model for li-ion batteries which takes into account the effect of SOC, temperature and storage duration. It predicts the rate of capacity loss given the total capacity loss at a given time in the storage lifetime of the battery (see (6)). The term k(T, SOC) is a function of temperature and SOC which is detailed in (7).

$$\frac{dQ_{cal}}{dt} = k(T, SOC) * \left(1 + \frac{Q_{cal}(t)}{Q_{nom}}\right)^{-\alpha(T)} \tag{6}$$

$$k(T, SOC) = k_A e^{-\frac{E_A}{R}\left(\frac{1}{T} - \frac{1}{T_{ref}}\right)} SOC + k_B e^{-\frac{E_B}{R}\left(\frac{1}{T} - \frac{1}{T_{ref}}\right)} \tag{7}$$

The studies outlined here mainly perform the testing for temperatures above 0C. The investigation performed in this work attempts to overcome this shortcoming by studying the effect of low temperature storage on the Li-ion battery capacity fade. Thus, three storage temperatures (-10, 40 and 60) and three storage durations have been chosen to investigate the effect on capacity degradation and later on the cycle ageing degradation rate. The further sections will focus on the experimental methodology, test matrices, modeling techniques and later present the testing results and go on to discuss them.

II. Experimental Methodology

A. Test vehicle

The test vehicles used for this investigation were two commercially available coin cells with cell A having a capacity of 90 mAh and a dimensionally larger cell B having a capacity of 120 mAh. Both cells featured the same cathode-anode chemistry (LiNiMnCoO2 (NMC) – graphite) and charge-discharge characteristics but differed in their capacity and dimensions. TABLE I summarizes the electrochemical properties of both the cells:

TABLE I. Physical Properties of Test Vehicles

Property	Cell A	Cell B
Nominal Capacity (mAh)	90	120
Nominal Voltage (V)	3.7	3.7
Operating Temperature (charging) (°C)	0 to 45	0 to 45
Operating Temperature (discharging) (°C)	-20 to 60	-20 to 60

TABLE II. Charge-Discharge Characteristics of Test Vehicles

Property	Cell A	Cell B
End of Charge Voltage (V)	4.2	4.2
Charge Current Range (mA)	45 (0.5C) to 180 (2C)	60 (0.5C) to 240 (2C)
End of Charge Current (mA)	1.7	2.4
End of Discharge Voltage (V)	3	3

For battery charging, a constant current-constant voltage (CCCV) charge profile was employed, while for discharge, a constant current profile was used. TABLE II enlists the manufacturer-specified charge-discharge profile characteristics for both the cells:

B. Experimental setup

For conducting the calendar ageing test of both the coin cells, the coin cells were subjected to three charge-discharge cycles so as to measure their initial capacity before storing them in a thermal chamber at the specified temperature and time. Combinations of three storage durations (1.5 months, 4 months, and 6 months) and three storage temperatures (-10°C, 40°C, and 60°C) were used to calendar age the cells. Two or more coin cells were aged and tested for every condition. After taking the cells out of storage, they were subjected to an accelerated charge-discharge cycling test as described in our previous work [11] (see Fig. 1).

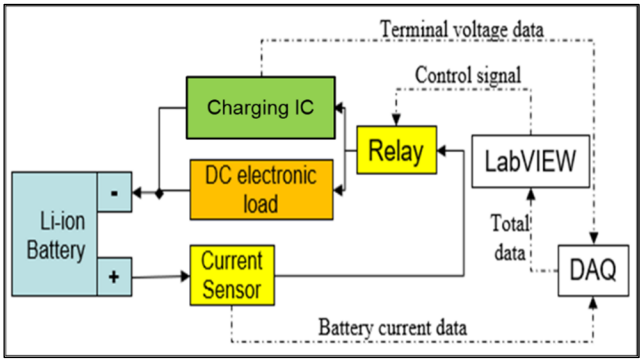

Fig. 1. Schematic Diagram of Test Setup

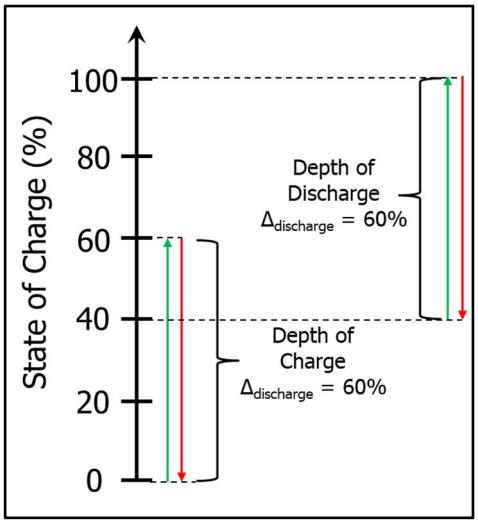

Fig. 2. Schematic of depth of charge and depth of discharge testing

As mentioned before, in this work, we subjected unaged coin cells to depth of discharge testing. In depth of discharge testing, the coin cell is charged completely (state of charge (SOC) 100%) and is then discharged by a specified percentage of the capacity followed by a full charge. This process is repeated for the desired number of cycles to degrade the battery. The depth of discharge test scheme is different from the depth of charge test scheme, as in depth of charge testing, the battery is discharged completely (0% SOC) and is then charged up to a desired SOC percentage. The battery SOH degradation caused by the depth of discharge testing is expected to be different than that caused by the depth of charge testing, as SOH degradation is a function of the battery voltage. Fig. 2 explains the nature of SOC variation between depth of charge and depth of discharge.

After the samples have been experimentally tested, the raw data is processed to determine the battery capacity and state of health, which are then plotted against the cycle number and utilized to construct a regression model. The formulas for calculating battery capacity (8) and SOH (9) are as follows:

$$Q = \sum (I_{discharge} * t_{sampling}) \tag{8}$$

$$SOH = \frac{Q_{n^{th}\ cycle}}{Q_{rated}} \tag{9}$$

For examining the effect of calendar ageing, the pre- and post-ageing battery capacities have been compared. The initial SOH values for all the samples tested are, however, normalized to 100% as it allows for easier comparison of the degradation slopes for different test settings while ignoring the pre-accumulated calendar aging effects.

C. Test Procedure and Matrices

For the battery samples that were subjected to calendar ageing, the accelerated life cycling tests after storage were performed with a 1.5C C-Rate for cell A and 2C C-rate for cell B. The discharge C-rate for all the tests was held constant at 1C and the operating temperature was maintained at 25°C. These charge-discharge and environmental use parameters were the same used for the depth of discharge testing. Table 1 and Table 2 summarize the calendar ageing tests and the depth of discharge tests respectively that were performed for both the cells.

TABLE III. TEST MATRIX FOR THE CALENDAR AGEING

Sr. No.	Cell Type	Storage Temperature	Storage Duration
1	1454/ 1654	-10	45, 120, 180
2		40	
3		60	

TABLE IV. TEST MATRIX FOR THE DEPTH OF DISCHARGE

Sr. No.	Cell Type	Depth of Discharge
1	1454/ 1654	50%
2		75%

D. Use Parameter-Based Regression Model Development

The empirical nonlinear regression model to be devised in this study relates the drop in capacity after ageing to the two calendar ageing parameters: storage temperature and duration. The model structure is simplistic and purely empirical with no physics-based degradation parameters being taken into account. One model each was developed for cell A and cell B. The general model form was as follows (10):

$$SOH = b_1 T_{ratio}^{b_2} D_{ratio}^{b_3} \tag{10}$$

The temperature ratio and the duration ratio are considered to normalize the model input parameters to reduce the variation in the model's output ((11) and (12)).

$$T_{ratio} = \frac{T_{Kelvin}}{298K} \tag{11}$$

$$D_{ratio} = \frac{D_{days}}{365 \text{ days}} \quad (12)$$

III. Results

The current section showcases the plots of the battery current and terminal voltage for both the test vehicles followed by their SOH degradation profiles under various testing conditions. The results are also presented in a comparative manner which makes it easy to study the effect of individual test parameters. However, the current section only deals with the presentation of the results obtained whereas their explanation and justification are included in the next section.

A. Battery Current and Terminal Voltage Plots

For cell A, graphs of battery current and terminal voltage for one discharge-charge cycle vs time for 1C D-rate and 1.5C C-rate are shown in Fig. 3. For the purpose of this research, the discharge current is negative and the charge current is positive. The CC discharge profile is followed by a CCCV charge profile, as seen in the annotations in Fig. 3. The same characteristics are plotted for cell B for 1C D-rate and 2C C-rate in Fig. 4.

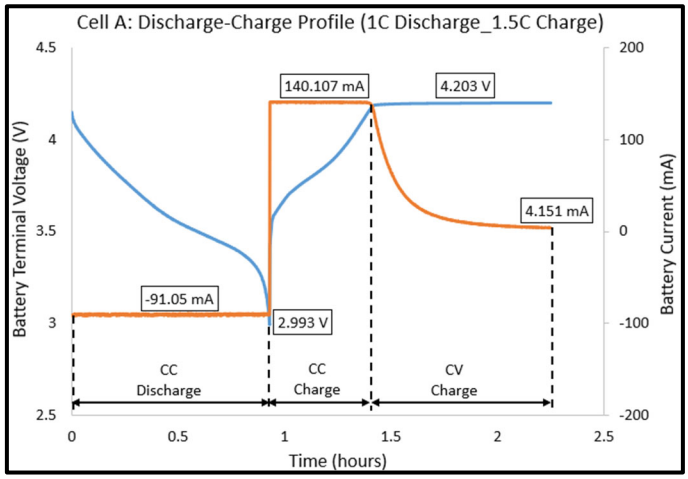

Fig. 3. Battery discharge-charge current and voltage profile for cell A

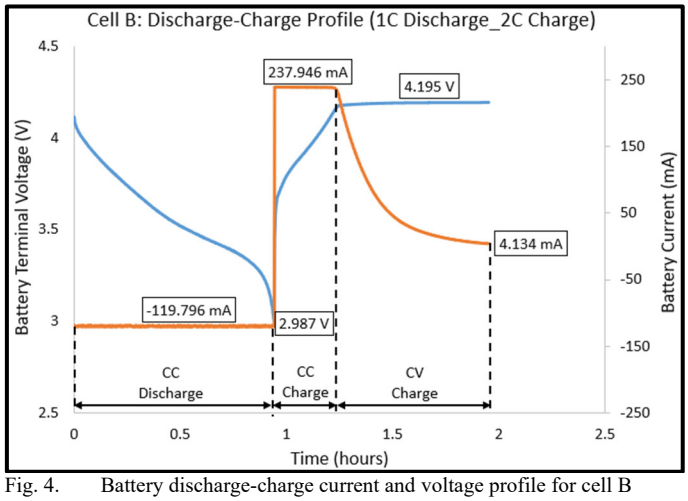

Fig. 4. Battery discharge-charge current and voltage profile for cell B

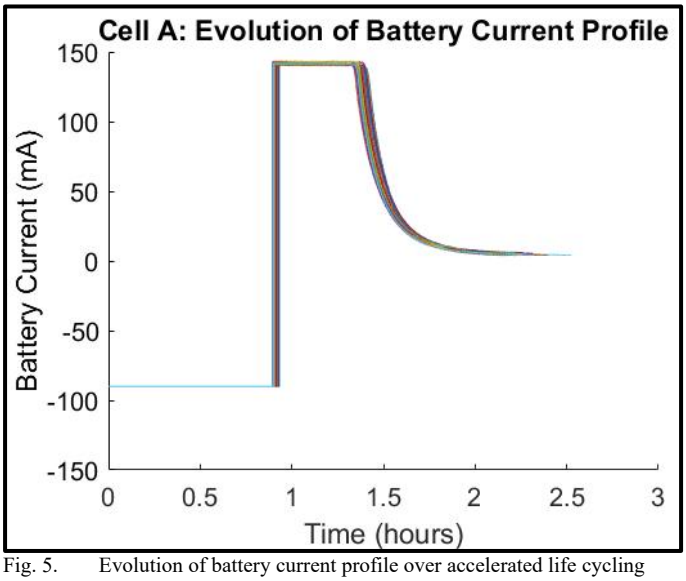

Fig. 5. Evolution of battery current profile over accelerated life cycling test for cell A

Finally, the evolution of the battery current and battery terminal voltage curves is plotted in Fig. 5 and Fig. 6 respectively for the full charge-discharge cycling of cell A at 1C D-rate and 1.5C C-rate for the entire duration of the accelerated life cycling test. As the C-D cycles increase, the current and the voltage curves shift leftwards indicating the reduced discharge time for the battery, which in turn is evidential of the battery SOH degradation.

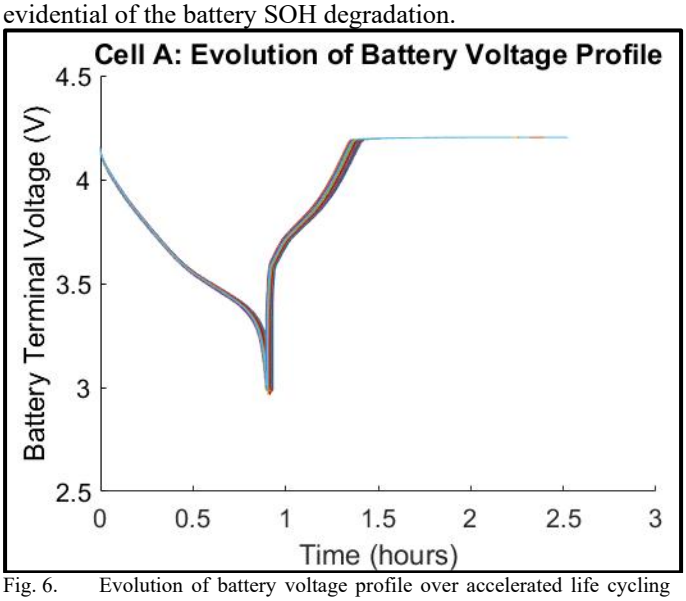

Fig. 6. Evolution of battery voltage profile over accelerated life cycling test for cell A

B. Comparison of Pre- and Post-Ageing Battery Capacity

This section presents the graphs of comparison of pre- and post-ageing battery capacity and thus depicts the effects of various storage durations and temperatures on the capacity drop. Fig. 7 shows a clustered bar graph representing the pre- and post-ageing capacity for cell A. Each cluster consists of two bars, the left one indicating the pre-ageing capacity and the right one indicating the post-ageing capacity. Owing to the plethora of storage temperature and duration combinations, the appropriate tests have been segregated and indicated on the graph itself. Following are the key takeaways from the graph:

(1) The cells stored at -10°C and 40°C don't show severe degradation in their pre- and post-ageing capacities. (2) With increasing storage duration, the capacity degradation due to storage increases only marginally for the cells stored at -10°C and 40°C. (3) The cells stored at 60°C show severe capacity degradation post ageing. (4) With increasing duration, the cells stored at 60°C show a very steep increase in capacity degradation. This capacity degradation behavior will be explained further with battery degradation physics in the discussion section.

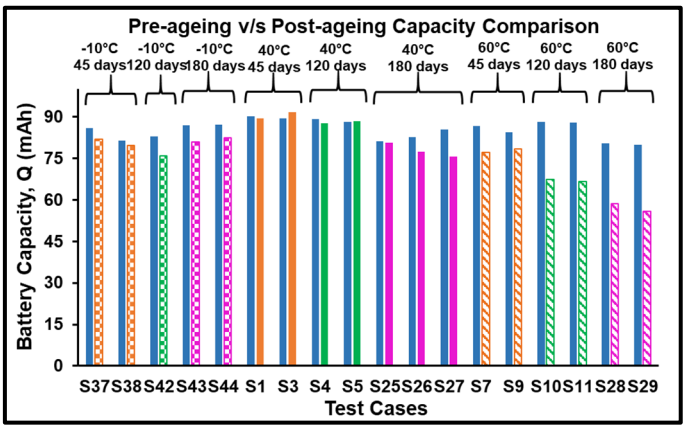

Fig. 7. Comparison of pre- and post-ageing capacities for calendar-aged samples of cell A

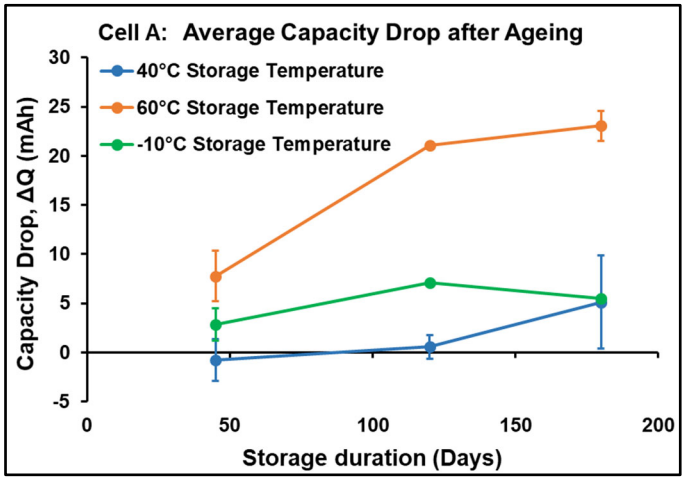

Fig. 8. Average capacity drop for cell A for various calendar ageing conditions

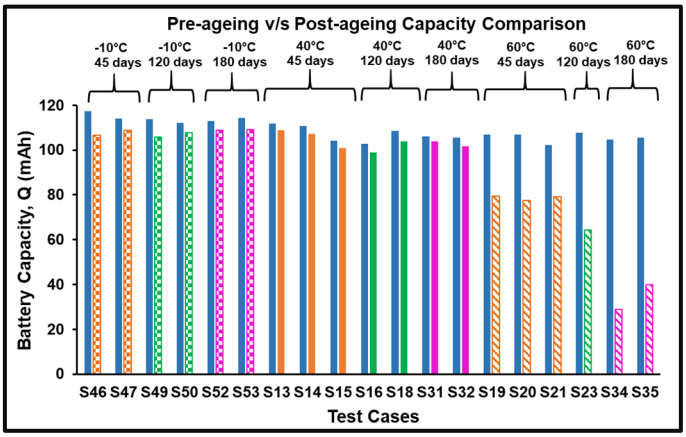

Fig. 9. Comparison of pre- and post-ageing capacities for calendar-aged samples of cell B

Fig. 8 plots the pre- and post-ageing capacity drop v/s the battery storage duration for different storage temperatures. This graph clearly summarizes the degradation behavior seen in Fig. 7. The capacity drops for the cells stored at -10°C and 40°C are lesser than those for the ones cycled at 60°C. Furthermore, the rate of increase of capacity drop with increasing duration is much steeper for the cells stored at 60°C than for the ones stored at -10°C or 40°C.

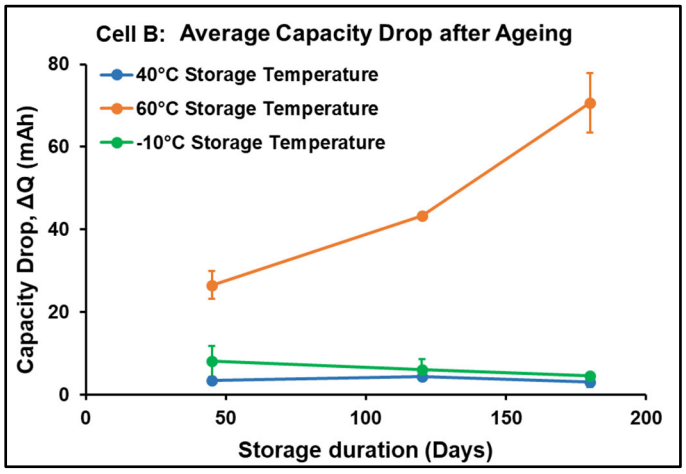

Fig. 10. Average capacity drop for cell B for various calendar ageing conditions

Fig. 9 and Fig. 10 show the same plots as Fig. 7 and Fig. 8 respectively for cell B. Furthermore, the degradation behaviors seen for cell A w.r.t. different storage durations and temperatures are similar to the ones that can be seen for cell B. This is again summarized in Fig. 10. The cells stored at -10°C and 40°C have much less calendar ageing drops which doesn't increase much with increase in storage durations. This, as opposed to the ones stored at 60°C, which have high capacity drops and also steep rate of increase with longer storage durations.

C. SOH Degradation: Effect of C-rate

This section presents the SOH degradation results with cyclic ageing of the battery samples which were earlier subjected to calendar ageing. Fig. 11 depicts the plots of cell A samples subjected to calendar ageing for various conditions that were later subjected to accelerated charge-discharge cycling.

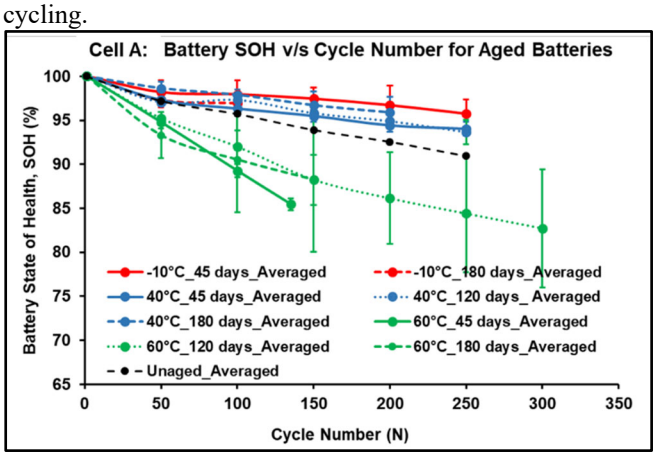

Fig. 11. Battery SOH v/s cycle number for calendar aged samples of cell A

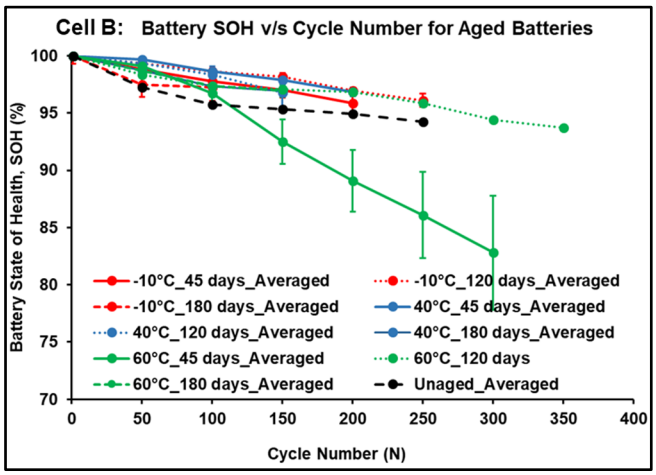

Fig. 12. Battery SOH v/s Cycle number for calendar aged samples of cell B

The black dashed line represents the SOH degradation of the unaged cell A sample which was subjected to the same cycle ageing parameters as the calendar aged cells. The red curves in the figure represent the cells aged at -10°C, the blue ones represent those aged at 40°C and the green ones are for those aged at 60°C. The line types (solid, dotted, dashed) represent the various storage durations. In general, it can be seen that, the cells aged at -10°C and 40°C have a SOH degradation rate for cycling which is similar to that of the unaged sample. On the other hand, the samples aged at 60°C have an SOH degradation rate which is steeper than the unaged one. Finally, the degradation rates for samples which are stored for shorter and longer durations have a negligible distinction. Thus, it can be concluded that, exposure of the cell to a 60°C environmental temperature leads to accelerated capacity drop in the battery. Fig. 12 shows the similar plot as Fig. 11 for the cell B samples which were subjected to cycle life ageing after their calendar ageing. The results for cell B are also similar to the ones seen for cell A.

E. SOH Degradation: Effect of Depth of Discharge

This section presents the results of the accelerated charge-discharge cycling on the battery samples to study the effect of depth of discharge. As mentioned in the methods section, two levels of depth of discharge, 50% and 75%, were investigated for this study. Fig. 13 and Fig. 14 show the SOH degradation vs. cycle number graphs for the cell A samples which were subjected to depth of discharge cycling and depth of charge cycling respectively. As can be seen from both the graphs, the depth of discharge plots have a higher degradation than the depth of charge plots for the same value of difference in SOC. This is expected as the battery sample experiences higher voltages during the depth of discharge test as compared to the depth of charge test. Also, the SOH degradation for the depth of discharge test is marginally lesser than that for the deep charge-discharge cycling test. Fig. 15 and Fig. 16 show similar plots as Fig. 13 and Fig. 14 respectively for cell B samples. The results for cell B are also similar to that of cell A where depth of discharge cycling leads to a higher degradation than the depth of charge cycling but lesser than full C-D cycling. This battery degradation behavior will again be explained in the discussion section.

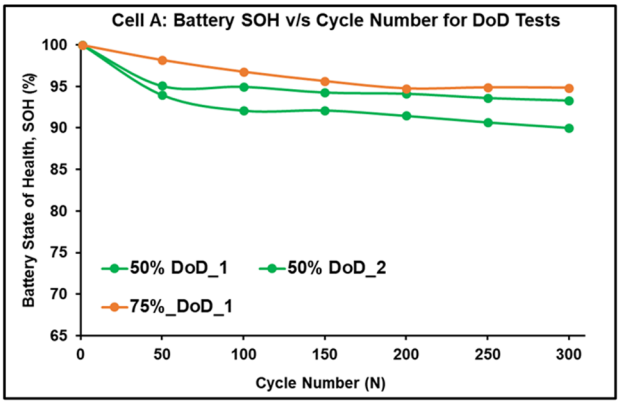

Fig. 13. Battery SOH v/s cycle number for depth of discharge testing for cell A

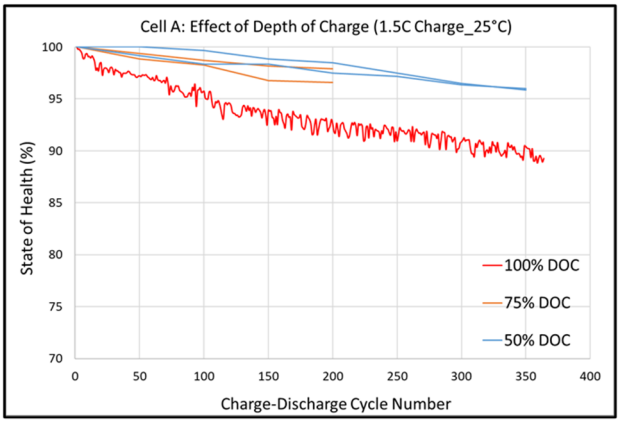

Fig. 14. Battery SOH v/s cycle number for depth of charge testing for cell A

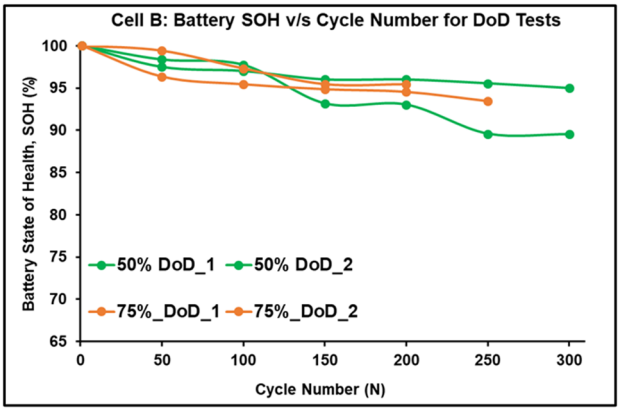

Fig. 15. Battery SOH v/s cycle number for depth of discharge testing for cell B

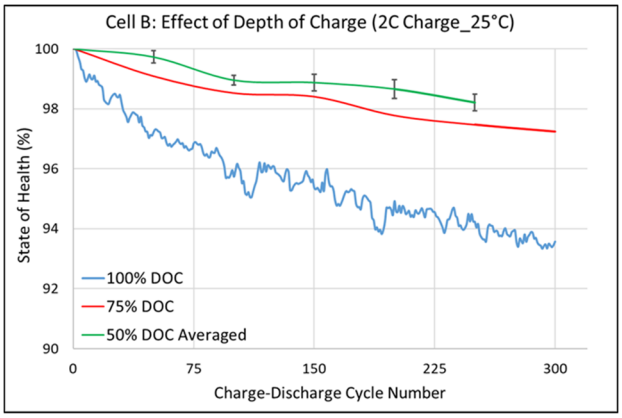

Fig. 16. Battery SOH v/s cycle number for depth of charge testing for cell B

F. Calendar Ageing Model

The state of health model equation and the generated experimental data for the pre- and post-ageing capacities of cell A and cell B were subjected to a nonlinear regression run on MATLAB. Following are the generated calendar ageing regression models for cells A (13) and B (14) respectively:

$$SOH = 1.88 T_{ratio}^{34.07} D_{ratio}^{1.11} \quad (13)$$

$$SOH = 0.76 T_{ratio}^{39.54} D_{ratio}^{0.48} \quad (14)$$

The R-Squared value and the RMS error for the calendar ageing model for cell A are 79.2% and 4.03% and those for cell B are 88.6% and 3.86% respectively.

IV. Discussion

The present section concentrates on the electrochemistry that underpins the deterioration patterns seen in both cell A and cell B during the experimentation phase. The creation of a Solid Electrolyte Interphase (SEI) film on the anode-electrolyte interface is commonly regarded in lithium-ion battery degradation literature as the principal source of capacity fading during long-term cycling [15]. The SEI layer is created as a result of a chemical reaction between the electrolyte and the anode surface, and its formation causes the electrolyte to decompose and cyclable Li+ ions to be consumed (see Fig. 17). Most of the degradation behaviors found in the current study are explained by the electrochemistry of SEI generation, which will be described in this section.

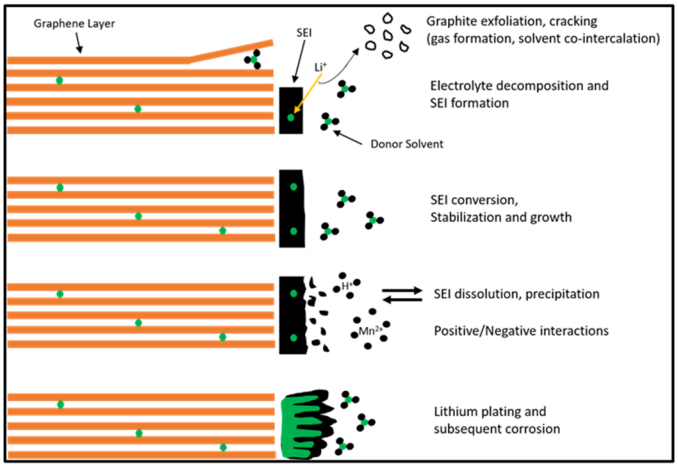

Fig. 17. Schematic of SEI initialization, growth, and subsequent Li-plating [15]

Kolzenberg [16] investigated the formation of SEI in Li-ion batteries and devised a physics-based model that explains the impact of depth of discharge on SOH deterioration. They discovered that the rate of SEI formation is proportional to the amount of neutral Li atoms present at the anode-electrolyte interface (see (15)).

$$j_{SEI} = \frac{c_{Li} D F^2 j_{\text{int}}}{2RT\kappa_{Li^+,SEI}} e^{-\eta_{SEI}} \quad (15)$$

In equation (15) j_{SEI} represents the rate of SEI formation, c_{Li} represents the concentration of lithium atoms at the anode-electrolyte interface, j_{int} is the intercalation rate of Li-ions in the anode which is equivalent to the charge C-rate, η_{SEI} is the overpotential for the SEI layer formation, $\kappa_{Li+,\ SEI}$ is the conductivity of the Li-ions in the SEI layer, T is the absolute operating temperature, and D, F, and R are the diffusion coefficient, Faraday constant and the universal gas constant, respectively. Now, as per the working of Li-ion batteries, during charging, the Li-ions migrate towards the anode due to which the Li atom concentration at the anode-electrolyte interface reduces, which in turn increases the rate of formation of SEI layer. Hence, during depth of discharge, when the Li-ion battery operates at higher voltages, more Li+ ions are present near the anode electrolyte interface leading to increased degradation. In equation (15) jSEI is the rate of SEI formation, cLi is the concentration of lithium atoms at the anode-electrolyte interface, j_{int} is the intercalation rate of Li-ions in the anode, which is equivalent to the charge C-rate, η_{SEI} is the overpotential for the SEI layer formation, $\kappa_{Li+,\ SEI}$ is the conductivity of the Li-ions in the SEI layer, T is the absolute operating temperature, and D, F, and R are the diffusion coefficient, Faraday constant and the universal gas constant, respectively. Due to the way Li-ion batteries work, the Li-ions migrate towards the anode during charging (corresponding to increased voltage), increasing the Li atom concentration at the anode-electrolyte interface, which speeds up the formation of the SEI layer. As a result, when the Li-ion battery works at higher voltages during depth of discharge, more Li^+ ions are present near the anode-electrolyte interface, causing enhanced degradation. Equation (15) shows an inverse relationship between SEI formation rate and absolute temperature, but increasing the temperature also changes other factors in the equation, leading in a trade-off. [17] suggests that the two parameters which strongly affect the calendar ageing of Li-ion batteries are high storage state of charge and high storage temperature. At higher temperatures, the thickness of the SEI layer at the anode is higher as compared to the unaged samples, which is an indicator of greater SOH degradation due to calendar ageing [6].

V. Summary and Conclusions

In this paper, the effect of calendar ageing with variation in storage duration and storage temperature is investigated for two coin cells. The cells were investigated for the difference in their pre- and post-ageing capacities. The findings of this study indicate that lower storage temperatures of -10°C and 40°C do not degrade the cells as much as higher storage temperature of 60°C. Also, with increased storage duration, the capacity degradation for cells stored at -10°C and 40°C shows marginal increase whereas that for 60°C shows steep increase. Furthermore, the calendar aged cells were later subjected to accelerated charge-discharge cycling and it was discovered that the samples aged at 60°C for both the cell types had a greater cyclic ageing rate as compared to those stored at lower temperatures. Furthermore, we also conducted the depth of discharge testing of pristine coin cells of types A and B. In both the cells it is seen that depth of discharge testing leads to higher capacity degradation as compared to that seen for depth of charge testing, but lower than that for deep cycling of the coin cells.

ACKNOWLEDGMENTS

The research results presented in this paper have been supported by members of NSF-CAVE3 Electronics Research Center.

REFERENCES

[1] X. Luo, J. Wang, M. Dooner, and J. Clarke, "Overview of current development in electrical energy storage technologies and the application potential in power system operation," *Appl. Energy*, vol. 137, pp. 511–536, January 2015.

[2] N. Nitta, F. Wu, J.T. Lee, and G. Yushin, "Li-ion battery materials: present and future," *Mater. today*, vol. 18, no. 5, pp. 252–264, June 2015.

[3] G. Zhou, F. Li, and H. Cheng, "Progress in flexible lithium batteries and future prospects," *Energy Environ. Sci.*, vol. 7, no. 4, pp. 1307-1338, November 2014.

[4] J.D. MacKenzie, and C. Ho, "Perspectives on energy storage for flexible electronic systems," *Proc. IEEE*, vol. 103, no. 4, pp. 535-553, April 2015.

[5] Y. Wang, B. Liu, Q. Li, S. Cartmell, S. Ferrara *et al.*, "Lithium and lithium ion batteries for applications in microelectronic devices: A review," *J. Power Sources*, vol. 286, pp. 330–345, July 2015.

[6] T. Waldmann, M. Wilka, M. Kasper, M. Fleischhammer, and M. Wohlfahrt-Mehrens, "Temperature dependent ageing mechanisms in Lithium-ion batteries – A Post-Mortem study," *J. Power Sources*, vol. 262, pp. 129–135, September 2014.

[7] L. Bodenes, R. Naturel, H. Martinez, R. Dedryvere, M. Menetrier *et al.*, "Lithium secondary batteries working at very high temperature: Capacity fade and understanding of aging mechanisms," *J. Power Sources*, vol. 236, pp. 265–275, August 2013.

[8] F. Leng, C.M. Tan, and M. Pecht, "Effect of Temperature on the Aging rate of Li Ion Battery Operating above Room Temperature," *Sci Rep.*, vol. 5**,** article no. 12967, February 2015.

[9] A. Tomaszewska, Z. Chu, X. Feng, S. O'Kane, X. Liu *et al.*, "Lithium-ion battery fast charging: A review," *eTransportation*, vol. 1, August 2019.

[10] Y. Li, K. Liu, A.M. Foley, A. Zulke, M. Berecibar *et al.*, "Data-driven health estimation and lifetime prediction of lithium-ion batteries: A review," *Renew. Sust. Energ. Rev.*, vol. 113, October 2019.

[11] P. Lall, V. Soni, G. Sethi. K. Yiang, "SOH modelling of Li-ion coin cells subjected to varying C-rates, depths of charge, operating temperatures and custom charge profiles," *20th IEEE ITherm*, pp. 634-643, 2021.

[12] R. Mingant, M. Petit, S. Belaid, J. Bernard, "Data-drive model development to predict the aging of a Li-ion battery pack in electric vehicles representative conditions," *J. Energy Storage*, vol. 39, pp. 1-11, 2021.

[13] E. Redondo-Iglesias, P. Venet, S. Pelissier, "Modelling lithium-ion battery ageing in electric vehicle applications – calendar and cycling ageing combination effects," *Batteries MDPI*, vol. 6, no. 1, pp. 14, 2020.

[14] O. Juhlin, "Modeling of battery degradation in electrified vehicles," 2016.

[15] M.M. Kabir, and D.E. Demirocak, "Degradation mechanisms in Li-ion batteries: a state-of-the-art review," *Int. J. Energy Res.*, vol. 41, no. 14, pp.1963– 1986, April 2017.

[16] L. von Kolzenberg, A. Latz, and B. Horstmann, "Solid-electrolyte interphase during battery cycling: theory of growth regimes," *Chem Sus Chem*, vol. 13, no. 15, article no. 3901, May 2020.

[17] P. Keil, S. Schuster, J. Wilhelm, J. Travi, A. Hauser, et al., "Calendar ageing of lithium-ion batteries," *J. Electrochem. Soc.*, vol. 163, no. 9, 2016.